

Sub-nanometer thin Conformal Aluminum Oxide Coating Created by Interconversion of SiO₂ *via* Hydrogen Plasma-assisted Atomic Layer Deposition

*Alex Henning^{§, +, *}, Johannes Bartl^{§, ‡, +}, Lukas Wolz[§], Maximilian Christis[§], Andreas Zeidler[§],
Michele Bissolo[§], Theresa Grünleitner[§], Johanna Eichhorn[§], Patrick Zeller^{†, #, %}, Matteo Amati[†],
Luca Gregoratti[†], Jonathan J. Finley[§], Bernhard Rieger[‡], Martin Stutzmann[§], Ian D. Sharp^{§, *}*

[§]Walter Schottky Institute and Physics Department, Technical University of Munich, 85748
Garching, Germany

[‡] Department of Chemistry, WACKER-Chair for Macromolecular Chemistry, Technische
Universität München, Lichtenbergstraße 4, 85747 Garching bei München, Germany

[†] Elettra-Sincrotrone Trieste SCpA, SS14-Km163.5 in Area Science Park, 34149, Trieste, Italy.

⁺These authors contributed equally

*sharp@wsi.tum.de, *alex.henning@wsi.tum.de

KEYWORDS Atomic layer deposition; Aluminum oxide, Silicon surface charge density, Field-
effect passivation

ABSTRACT We present a route towards ultrathin and continuous aluminum oxide (AlO_x) coatings on silicon substrates for the spatial control of the charge density. X-ray photoelectron spectroscopy provides strong indication for the chemical reduction of SiO_2 and its transformation into AlO_x following exposure to trimethylaluminum and hydrogen plasma. Tailoring the growth parameters of plasma-assisted atomic layer deposition allows to achieve partial conversion of SiO_2 , resulting in ~ 0.4 nm thin continuous AlO_x coatings that can be deposited at low-temperatures (70 °C) in selected regions defined by lithographic patterning. We envision applications for local gating, carrier selective contacts in silicon solar cells and selective surface functionalization.

INTRODUCTION

Atomic layer deposition (ALD) of amorphous alumina (AlO_x) is widely applied in silicon (Si) technology, including for the dielectric and chemical passivation,^{1, 2} carrier-selective charge transfer at the interfaces in Si solar cells,³⁻⁵ as a gate dielectric in non-planar field-effect transistors, as well as a diffusion barrier and protective coating. ALD AlO_x introduces a high density of negative fixed charges in the range of 10^{12} – 10^{13} cm^{-2} ,⁶ which repel electrons from the silicon surface, suppressing surface recombination *via* field-effect and improving the efficiency of Si solar cells.^{1, 6, 7} More recently, ultrathin AlO_x has been implemented as an interlayer for hole-selective tunnel contacts in *p*-doped Si further improving the performance of Si solar cells.^{5, 8-10}

Notably, it has been demonstrated that several ALD AlO_x monolayers have the same potential for field-effect passivation as thicker AlO_x films on *p*-doped Si.^{2, 10-12} Other related studies unveiled that the coordination and bonds at the $\text{SiO}_x/\text{AlO}_x$ interface predominantly govern interface state density and negative charges, whereas the coordination remains unchanged away from the interface.^{6, 13} Thus, a sub-nanometer thin AlO_x coating that introduces fixed charges and

enhances charge carrier tunneling can further reduce impedance and improve carrier selectivity at *p*-doped Si contact interfaces. However, up to date, sub-nanometer thin and conformal ALD coatings are challenging to achieve due to steric effects and available binding sites, leading to three-dimensional island growth during the nucleation regime.² In fact, it has been shown that a significantly lower negative fixed charge is introduced at the Si/SiO₂/AlO_x interface for few cycle ALD processes¹⁰ because the synthesized AlO_x films are likely discontinuous.¹²

Here we applied plasma-assisted ALD for the growth of ~0.4 nm thin conformal coatings *via* oxide conversion, to define smooth dielectric environments for the control of the surface charge density. Thereby, the surface oxide on Si provides the oxygen atoms for the growth of AlO_x following alternating exposure to trimethylaluminum (TMA) and remote hydrogen (H₂) plasma. By omitting the use of a gas-phase oxidant during ALD, we show that the SiO₂ layer thickness decreases, whereas it increases for standard ALD AlO_x processes using H₂O and oxygen-plasma,^{12, 14} the latter of which generates defects and introduces detrimental interface states.¹⁵ Therefore, by applying the TMA/H₂ process, ultrathin (and high-quality) SiO₂/AlO_x dielectric layers in the regime of electron tunneling are achieved. Moreover, the TMA/H₂ process is compatible with temperatures below 100 °C and thus with lift off processing. The demonstrated AlO_x charge density micropatterns provide an intriguing possibility for carrier selective contacts in Si solar cells, selective surface functionalization¹⁶ and local gating.

RESULTS AND DISCUSSION

I. Native SiO₂ conversion to AlO_x following exposure to H₂ plasma and trimethylaluminum. To gain mechanistic insights into the growth of AlO_x on Si with TMA and remote H₂ plasma without the use of a gas-phase oxygen source, we tracked the ALD film

thickness in real-time by *in situ* spectroscopic ellipsometry (SE) and assessed the chemical composition by X-ray photoelectron spectroscopy (XPS). The evolution of the AlO_x growth, derived from SE (**Fig. 1a**), reveals a decrease in the growth rate after ~ 20 cycles (at 200°C), indicating consumption of the available binding sites (*i.e.*, Si-O-H and Si-O groups) on the moderately hydrophilic silicon surface covered by a $\sim 16\text{ \AA}$ thick native SiO_2 (Table S1). In this regard, the inflection point of the growth rate, which is derived from the thickness change, corresponds to the minimum number of cycles required to achieve a complete surface coverage. The different growth rates suggest distinct growth regimes (denoted as i and ii in Fig. 1a), in which different surface chemical reactions dominate. X-ray photoelectron spectra confirm the presence of a native SiO_2 layer on the silicon substrate prior to ALD (Fig. 1b). Following 5 cycles of TMA and H_2 plasma (100 W power), the component of the Si 2p core level spectrum at a binding energy (BE) of $\sim 103\text{ eV}$, attributed to SiO_2 (Si^{4+}), decreased in intensity while additional spectral features at relatively lower BEs ($< 103\text{ eV}$) emerged, revealing the formation of a SiO_x ($x < 2$) sub-oxide on the substrate surface during the TMA/ H_2 plasma process (Fig. 1b). We note that sub-stoichiometric transition layers are commonly present at Si/ SiO_2 interfaces;¹⁷ however, we focus our analysis on changes in the SiO_x sub-oxide species following ALD. Concomitantly, the overall intensity of the emitted photoelectrons from the Si 2p spectral region decreased, while simultaneously an aluminum (Al 2p) component at the characteristic BE of Al-O environment ($\sim 75.5\text{ eV}$) emerged (Fig. 1b, inset). Thus, XPS confirmed the formation of an alumina layer on Si substrate after the TMA/ H_2 plasma process. In addition, the appearance of sub-stoichiometric SiO_x after the ALD process indicates a reduction of the surface SiO_2 . The concurrent appearance of sub-stoichiometric SiO_x (Fig. 1b) and an alumina component (Al 2p) at a relatively low peak BE of $\sim 75.0\text{ eV}$ following 5 cycles TMA/ H_2 plasma (Fig. 1b, inset) suggest the formation of a mixed phase (*i.e.*,

Si-O-Al bonding), although the creation of oxygen-deficient SiO_x with oxygen vacancies cannot be excluded from the XPS spectra. From the combined insights gained by SE and XPS, we infer that hydrogen plasma and TMA chemically react with the oxidized substrate surface until saturation of bindings sites (and depletion of surface oxygen), thereby partially transforming the native SiO_2 into AlO_x , which is consistent with previously predicted redox reaction of TMA with SiO_2 based on thermodynamic considerations ($\Delta G = -235 \text{ kcal/mol}$ at 300°C).¹⁸ Notably, the ultrathin alumina coating that formed after several cycles substantially reduced the work function (Fig. S1) and altered the surface chemistry resulting in a more hydrophilic surface, as indicated by the reduction in the static water contact angle from initially 64° for the bare Si substrate to 25° for the TMA/ H_2 plasma treated Si (Table S1). This can be exploited for subsequent chemical functionalization of the AlO_x -terminated surface, as recently reported by our group.^{19, 20} We next turn our attention to growth regime (ii) (Fig. 1a), in which film deposition proceeded at a constant rate despite the absence of an oxygen source. After 200 cycles of TMA and H_2 plasma, the native SiO_2 layer on Si is reduced to SiO_x suboxides, leaving a surface coated with AlO_x , and a top layer consisting of aluminum carbide (AlC_x) (Fig. S2). We note that the formation of an AlSi_xO_y interfacial layer has been reported for the direct deposition of ALD AlO_x on Si, albeit for annealed samples.¹³ In this study, we found no clear evidence for AlSi_xO_y .

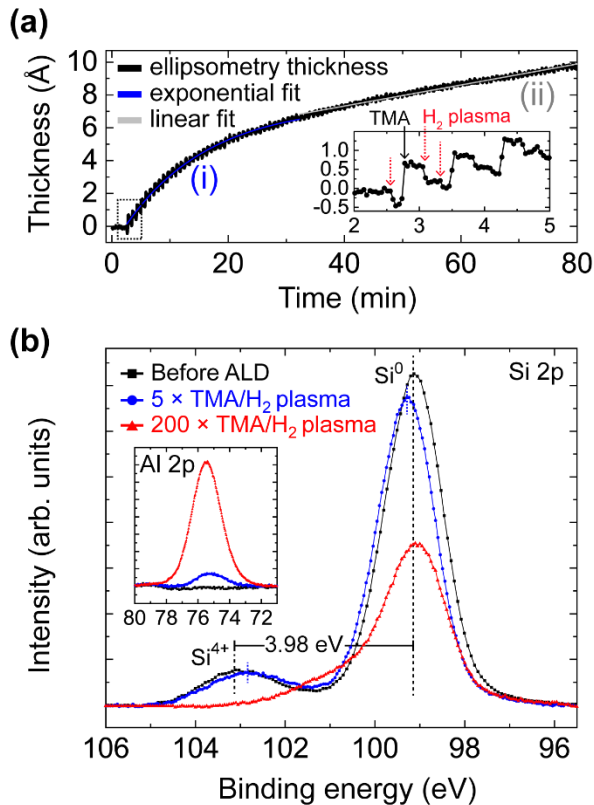


Figure 1. (a) Evolution of the AlO_x thickness, derived from *in situ* SE is shown for 100 cycles of consecutive exposure to TMA and H₂ plasma (100 W) and 200 °C. (b) AlO_x created by TMA/H₂ plasma process on a Si substrate with native SiO₂. XPS shows that the ratio between elemental Si, denoted as Si(0), and SiO₂ (Si⁴⁺) decreased already after 5 cycles of TMA and H₂ plasma. The spectra were recorded at a pass energy (PE) of 20 eV.

To increase the growth rate and deposit thicker films on Si substrates during growth regime (ii) (Fig. 1a), we used a higher plasma power (300 W) (**Fig. 2**). XPS analysis revealed the deposition of elemental aluminum (Figs. 2a and S3) after prolonged exposure to TMA/H₂ (200 cycles, 300 W plasma power), consistent with a previous report.²¹ Concurrently, an aluminum carbide component at a BE characteristic of Al₄C₃ appears in the core level spectra of Al 2p (Fig. 2b) and C 1s (Fig. S4).²²

In addition, X-ray photoelectron spectra demonstrate that the native SiO₂ layer on Si was entirely reduced to elemental Si after 200 cycles of the TMA/H₂ plasma process at 300 W plasma power (Fig. 2b). Such complete transformation of the ~16 Å thick SiO₂ layer into AlO_x (and potentially AlSi_xO_y), as well as the observed decrease in the XPS intensity ratio, I(Si 2p):I(Al 2p), of both elements (Fig. 1b) imply transport of oxygen through the SiO₂ film to the surface or interface. The activation energy for the diffusion of molecular oxygen through SiO₂ has been predicted by density function theory to be 0.3 eV,²³ which is lower than the reported activation energy of aluminum diffusion in amorphous SiO₂ of 0.73 eV.²⁴ Although the growth temperature of 200 °C (0.041 eV) is below the diffusion activation energies of both elements, it is far more likely for oxygen than for Al to diffuse within SiO₂. We hypothesize that the oxygen in the SiO₂ layer is extracted by the strongly reducing Al or AlC_x surface layer that is likely formed following reduction of the surface oxides (SiO₂, AlSiO_x, AlO_x) by TMA and the reactive species (*e.g.*, H⁺) of the H₂ plasma. The gradient in the reduction potential facilitates the migration of oxygen to the surface, where it reacts to AlO_x. Cyclic exposure to TMA and remotely generated H₂ plasma perpetuates the repetitive surface layer reduction and oxidation. By increasing the plasma power, increases the fraction of ionized species reaching the sample surface and enhances the formation rate of the reduced surface layer, which can explain the relatively stronger reduction of SiO₂ and deposition of elemental Al (Fig. 2). According to the proposed growth model, the extent of the “oxygen reservoir” of the substrate is expected to affect the growth behavior. Indeed, we observed a faster growth rate with a slower decay on a Si substrate coated with thermal SiO₂ (Fig. S5) than on a Si substrate with native SiO₂ (Fig. 1a).

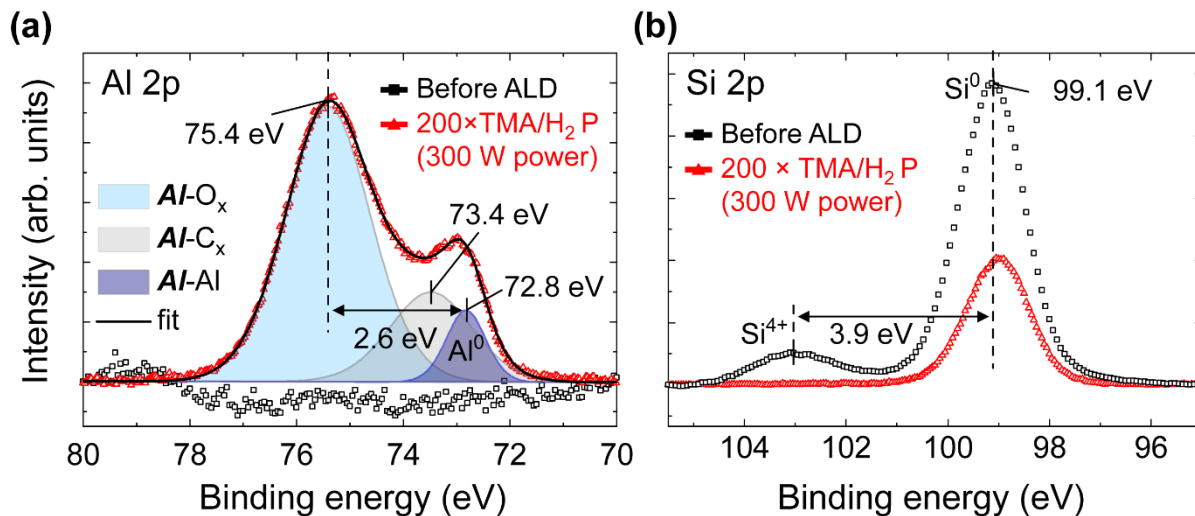


Figure 2. XPS spectra of (a) the Al 2p and (b) Si 2p spectral regions of a Si substrate before and after treatment with 200 cycles of the TMA/H₂ plasma process at 300 W plasma power and 200 °C.

II. AlO_x can be conformally deposited with sub-nanometer thickness and introduces negative charges at the SiO_x/AlO_x interface. Owing to the high reactivity of both TMA and H₂ plasma, the ALD process is compatible with temperatures below 100 °C and thus with lithographic processing, which we exploited to create a micropattern (**Fig. 3**). Scanning electron microscopy (SEM) and scanning photoelectron microscopy (SPEM) depict the AlO_x pattern on the doped Si substrate (Figs. 3 a,b).

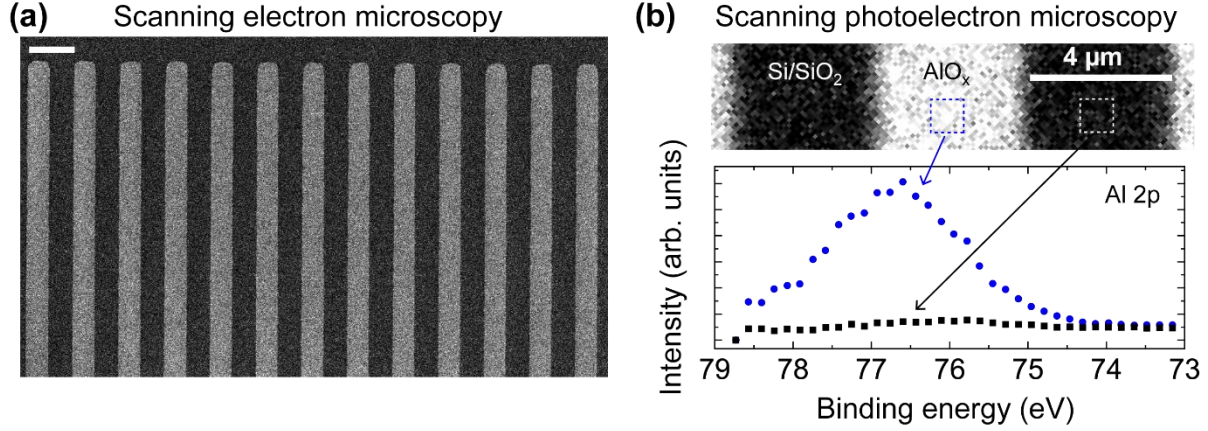


Figure 3. (a) Secondary electron scanning electron microscopy image of an AlO_x pattern on Si substrate following 20 cycles of TMA and H₂ plasma at 70 °C. (b) Synchrotron-based scanning photoelectron microscopy map of the Al 2p core level. Every pixel (150 × 150 nm²) represents a spectrum of the kinetic energy in the range from 559 – 565 eV corresponding to a BEs from 79 – 73 eV. The sample was excited with photons of 638 eV energy. The photoelectron core level spectra (bottom) were retrieved from the marked square regions in the SPEM image.

We determined the AlO_x thickness and the surface potential on both surfaces from the atomic force microscopy (AFM) and Kelvin probe force microscopy maps of the AlO_x pattern on the Si substrate (**Fig. 4**). Both the topography and the simultaneously acquired contact potential difference (CPD) maps are uniform within each region, demonstrating a continuous AlO_x coating. The profile extracted from the AFM topograph (Fig. 4c, top) shows a height difference between the uncoated and AlO_x-covered Si region of 4 ± 0.3 Å, which is thinner than previously reported for conformal ALD AlO_x coatings on Si. Notably, both surfaces are smooth exhibiting an rms roughness (R_{rms}) of 0.18 nm (determined from a 2×2 μm² scan, 512 points sampling, ~10 nm tip radius of Si tip) (Fig. 4a, c). The fact that the surface remains smooth after the TMA/H₂ plasma process is an important criterion for its implementation in semiconductor technology processing. The potential profile across the patterned region reveals an abrupt potential step of ~0.42 V,

yielding an electric field of $\sim 3 \text{ V}/\mu\text{m}$ at the lateral interface between bare and AlO_x -coated p-doped Si (Fig. 4c, bottom) whose magnitude is determined by the photolithography process and experimentally underestimated due to the finite tip radius of the platinum-iridium-coated Si tip of about $\sim 30 \text{ nm}$. Importantly, the surface potential difference is maintained over several months in ambient (Fig. S5).

The measured decrease in the CPD following deposition of the 0.4 nm thin AlO_x layer can be explained with the formation of a microscopic surface dipole, whose negative charges at the $\text{SiO}_2/\text{AlO}_x$ interface⁶ are compensated by the positive charges from the AlO_x coated surface ($Q_{\text{surface}} = Q_{\text{interface}}$). Thus, a microscopic dipole layer with its positive end pointing outwards leads to the observed decrease in the CPD and work function. For comparison, we also characterized *n*-doped Si and observed a similar potential step (i.e., $\sim -0.4 \text{ V}$ CPD decrease after the TMA/ H_2 plasma process), indicating that the surface band bending of highly doped Si remains greatly unchanged after ALD. This observation is consistent with earlier reports revealing Fermi level pinning of doped Si by interface and surface states.²⁵ We conclude that the observed CPD decrease after formation of the ultrathin AlO_x layer is mainly caused by charge redistributions in the surface oxide layers.

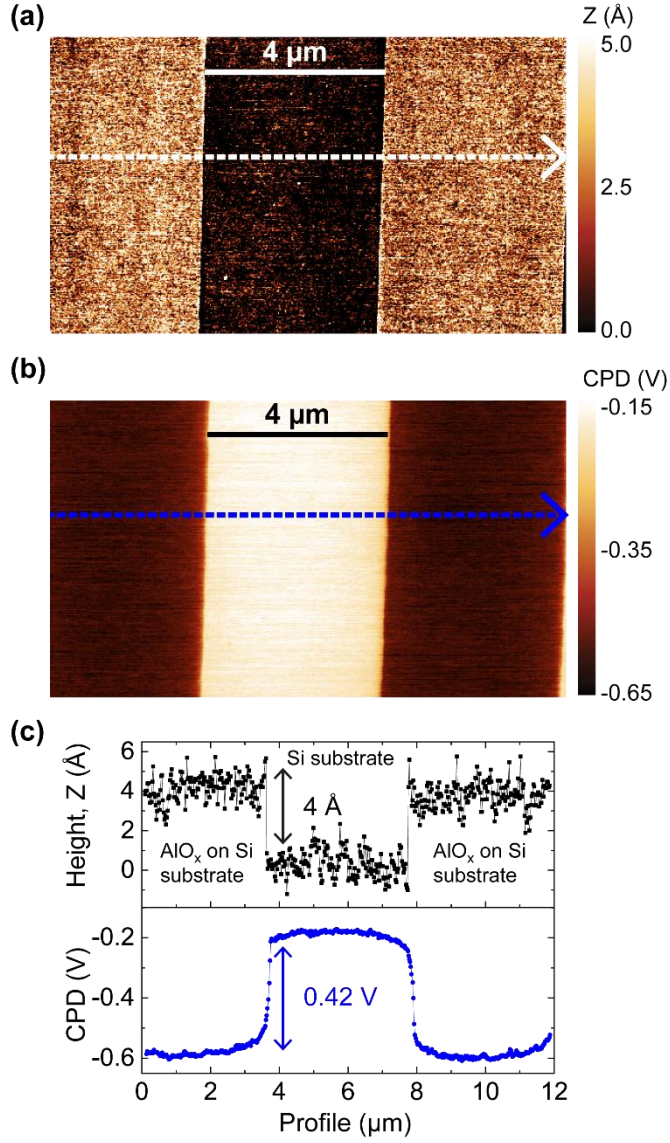


Figure 4. (a) Intermittent contact mode AFM topography and (b) frequency modulation KPFM image of the AlO_x pattern on Si substrate. (c) Topography and CPD profiles were taken along the lines as indicated in the images of a and b.

CONCLUSION

In summary, we presented an ALD process based on TMA and remote hydrogen plasma for the realization of sub-nanometer thin continuous AlO_x coatings on silicon. The conformal AlO_x layer can be lithographically patterned to locally modify the dielectric environment and surface chemistry. We envision that the presented gas-phase processing concept finds application for the surface functionalization of (bio)chemical sensors, reduction of the contact resistance of hole-selective Si contacts, the field-effect passivation of Si and defining spatially controlled gates.

MATERIALS AND METHODS

Si Substrate properties. Highly *n*-doped (Arsenic) and *p*-doped (Boron) Si substrates (Sievert Wafer, Germany) with a <100> crystal orientation and a resistivity of $\sim 0.005 \, \Omega \, \text{cm}$ were used. The surfaces were chemo-mechanically polished on one side by the manufacturer. Silicon substrates with a $\sim 1.8 \, \text{nm}$ thick native silicon dioxide layer or with a $270 \, \text{nm}$ thick thermal SiO_2 were analyzed. The thicknesses of the oxide layers were determined by SE.

Optical lithography. Lithographic lift-off processing was combined with low-temperature plasma-assisted ALD to define a micropattern of AlO_x on a Si substrate. A resist double layer consisting of poly-dimethyl glutarimide (PMGI SF3, Microchem) and ma-P 1205 (micro resist technology) was patterned with a maskless aligner (Heidelberg, MLA100) and developed in tetramethylammonium hydroxide (TMAH, micro resist technology). Lift-off was performed by ultrasonication (10 min, $40 \, ^\circ\text{C}$) in *n*-methyl-2-pyrrolidone (NMP, micro resist technology).

Atomic layer deposition. Plasma-assisted ALD was carried out in a hot wall reactor (Fiji G2, Veeco) at either $200 \, ^\circ\text{C}$ or $70 \, ^\circ\text{C}$ using argon (99.9999 %, Linde) as the carrier and purge gas. A

~0.4 nm thick aluminum oxide film was formed on the Si substrate following 20 cycles of sequential exposure to TMA (Strem) and remote hydrogen plasma (100 W, 2 s) that was generated with a sapphire-based inductively coupled plasma source. The purge times in argon (110 sscm, 0.09 Torr) after every half-cycle were 15 s. Because the native SiO₂ layer of the silicon substrate served as the oxygen source the growth rate decreased exponentially.

We note that cleaning Si surfaces with hydrogen plasma (100 W, 20 sscm, 0.3 Torr) removes adventitious organic contamination and activates the surface.²⁶ However, hydrogen ions generated from a remote plasma may also increase the number of interface states in Si(100).²⁷

Spectroscopic ellipsometry. We obtained the thickness of the SiO₂ layers and the ALD AlO_x film by analyzing the ellipsometry spectra with established optical models for silicon and SiO₂ and by using a Cauchy model for the AlO_x layer.

X-ray photoelectron spectroscopy. XPS measurements were performed with a custom-built system utilizing components from SPECS Surface Nano Analysis GmbH (Germany), a twin (Al and Mg) non-monochromatic X-ray tube anode, a PHOIBOS 100 concentric hemispherical analyzer, and a MCD-5 detector. Measurements were performed at a base pressure below 7×10^{-9} mbar. The Al X-ray source (Al K _{α} = 1486.6 eV) was operated at an emission current of 20 mA with a voltage of 12.5 kV. XPS spectra were recorded with a pass energy of 20 eV or 10 eV in normal emission ($90^\circ \pm 2^\circ$ relative to the surface) in medium area mode (circular electron collection area of 2 mm diameter). Measurement parameters are transmission optimized, resulting in an acceptance angle up to $\pm 7^\circ$. With these settings an instrumental resolution of 1.2 eV was determined by measuring the full width at half maximum (FWHM) of a gold (Au) 4f_{7/2} XPS spectrum recorded on a 100 nm Au layer evaporated on a Si(100) wafer die. The binding energy

of the hemispherical analyzer was calibrated with silver and gold standard samples. Thereby, the kinetic energies of the Ag 3d (1118.51 eV), Au 4f (1402.73 eV) and Cu 2p (554.07 eV) core levels were referenced to the known peak values. XPS spectra were recorded with SpecsLab (SPECS Surface Nano Analysis GmbH, ver. 2.85).

Scanning photoelectron microscopy (SPEM). Synchrotron-based SPEM measurements were performed at the ESCA microscopy beamline at the Elettra synchrotron (Trieste, Italy). Technical details of the SPEM setup is described elsewhere.²⁸ The X-ray photon energy was set to 638 eV with a (Gaussian) X-ray focal radius of ~150 nm and a pass energy (PE) of 20 eV, resulting in an instrumental broadening of 0.35 eV determined by the Au 4f from an internal gold standard. Maps were acquired by using a multichannel delay line detector, allowing the acquisition of a spectrum in snap-shot mode at every pixel of the map.

ASSOCIATED CONTENT

Supporting Information. The following files are available free of charge.

Supporting static water contact angle measurements. Additional AFM and XPS data (PDF)

AUTHOR INFORMATION

Corresponding Author

*sharp@wsi.tum.de, *alex.henning@wsi.tum.de

Present Addresses

#Helmholtz-Zentrum Berlin für Materialien and Energie GmbH, BESSY II, Albert-Einstein-Straße 15, 12489 Berlin, Germany

% Fritz-Haber-Institut der Max-Planck-Gesellschaft, Dept. Inorganic Chemistry, Faradayweg 4-6, 14195 Berlin, Germany

Author Contributions

All authors have given approval to the final version of the manuscript. [†]These authors contributed equally.

Funding Sources

AH acknowledges funding from the European Union's Horizon 2020 research and innovation programme under the Marie Skłodowska-Curie grant agreement No 841556.

ACKNOWLEDGMENT

We greatly acknowledge support from Claudia Paulus.

REFERENCES

1. Schmidt, J.; Merkle, A.; Brendel, R.; Hoex, B.; de Sanden, M. C. M. v.; Kessels, W. M. M. *Progress in Photovoltaics: Research and Applications* 2008, 16, (6), 461-466.
2. Naumann, V.; Otto, M.; Wehrspohn, R. B.; Hagendorf, C. *Journal of Vacuum Science & Technology A* 2012, 30, (4), 04D106.
3. Xin, Z.; Ling, Z. P.; Nandakumar, N.; Kaur, G.; Ke, C.; Liao, B.; Aberle, A. G.; Stangl, R. *Japanese Journal of Applied Physics* 2017, 56, (8S2), 08MB14.
4. Liu, K.; Cristini-Robbe, O.; Elmi, O. I.; Wang, S. L.; Wei, B.; Yu, I.; Portier, X.; Goubilleau, F.; Stiévenard, D.; Xu, T. *Nanoscale Research Letters* 2019, 14, (1), 330.
5. Xin, Z.; Ling, Z. P.; Wang, P.; Ge, J.; Ke, C.; Choi, K. B.; Aberle, A. G.; Stangl, R. *Solar Energy Materials and Solar Cells* 2019, 191, 164-174.
6. Simon, D. K.; Jordan, P. M.; Mikolajick, T.; Dirnstorfer, I. *ACS Applied Materials & Interfaces* 2015, 7, (51), 28215-28222.
7. Damianos, D.; Vitrant, G.; Kaminski-Cachopo, A.; Blanc-Pelissier, D.; Ghibaudo, G.; Lei, M.; Changala, J.; Bouchard, A.; Mescot, X.; Gri, M.; Cristoloveanu, S.; Ionica, I. *Journal of Applied Physics* 2018, 124, (12), 125309.
8. Davis, B. E.; Strandwitz, N. C. *IEEE Journal of Photovoltaics* 2020, 10, (3), 722-728.
9. Ögütman, K.; Iqbal, N.; Gregory, G.; Li, M.; Haslinger, M.; Cornagliotti, E.; Schoenfeld, W. V.; John, J.; Davis, K. O. *physica status solidi (a)* 2020, 217, (18), 2000348.
10. Hiller, D.; Göttlicher, J.; Steininger, R.; Huthwelker, T.; Julin, J.; Munnik, F.; Wahl, M.; Bock, W.; Schoenaers, B.; Stesmans, A.; König, D. *ACS Applied Materials & Interfaces* 2018, 10, (36), 30495-30505.
11. Terlinden, N. M.; Dingemans, G.; Sanden, M. C. M. v. d.; Kessels, W. M. M. *Applied Physics Letters* 2010, 96, (11), 112101.
12. Werner, F.; Veith, B.; Zielke, D.; Kühnemund, L.; Tegenkamp, C.; Seibt, M.; Brendel, R.; Schmidt, J. *Journal of Applied Physics* 2011, 109, (11), 113701.
13. Kim, K.; Nandakumar, N.; Zheng, X.; Lim, S.; Hameiri, Z. *IEEE Journal of Photovoltaics* 2021, 11, (3), 620-626.
14. Fukumizu, H.; Sekine, M.; Hori, M.; McIntyre, P. C. *Japanese Journal of Applied Physics* 2020, 59, (1), 016504.
15. Min, K. H.; Choi, S.; Jeong, M. S.; Kang, M. G.; Park, S.; Song, H.-e.; Lee, J. I.; Kim, D. *Current Applied Physics* 2019, 19, (2), 155-161.
16. Blaschke, D.; Pahlow, S.; Fremberg, T.; Weber, K.; Müller, A. D.; Kurz, S.; Spohn, J.; Dhandapani, V.; Rebohle, L.; Skorupa, I.; Schmidt, H. *Applied Surface Science* 2021, 545, 148729.
17. Himpfel, F. J.; McFeely, F. R.; Taleb-Ibrahimi, A.; Yarmoff, J. A.; Hollinger, G. *Physical Review B* 1988, 38, (9), 6084-6096.
18. DuMont, J. W.; Marquardt, A. E.; Cano, A. M.; George, S. M. *ACS Applied Materials & Interfaces* 2017, 9, (11), 10296-10307.

19. Henning, A.; Bartl, J. D.; Zeidler, A.; Qian, S.; Bienek, O.; Jiang, C.-M.; Paulus, C.; Rieger, B.; Stutzmann, M.; Sharp, I. D. *Advanced Functional Materials* 2021, 31, (33), 2101441.
20. Liu, K. S.; Henning, A.; Heindl, M. W.; Allert, R. D.; Bartl, J. D.; Sharp, I. D.; Rizzato, R.; Bucher, D. B. *arXiv preprint arXiv:2103.15955* 2021.
21. Lee, Y. J.; Kang, S.-W. *Electrochemical and Solid-State Letters* 2002, 5, (10), C91.
22. Hauert, R.; Patscheider, J.; Tobler, M.; Zehring, R. *Surface Science* 1993, 292, (1), 121-129.
23. Hoshino, T.; Hata, M.; Neya, S.; Nishioka, Y.; Watanabe, T.; Tatsumura, K.; Ohdomari, I. *Japanese Journal of Applied Physics* 2003, 42, (Part 1, No. 6A), 3560-3565.
24. Berry, W. B.; Emery, K. A.; Swartzlander, A. B.; Nelson, A. J. In *Low temperature diffusivity for aluminum and silver in amorphous silicon*, Conference Record of the Twentieth IEEE Photovoltaic Specialists Conference, 26-30 Sept. 1988, 1988; pp 262-266 vol.1.
25. Arita, M.; Torigoe, K.; Yamauchi, T.; Nagaoka, T.; Aiso, T.; Yamashita, Y.; Motooka, T. *Applied Physics Letters* 2014, 104, (13), 132103.
26. Gupta, V.; Madaan, N.; Jensen, D. S.; Kunzler, S. C.; Linford, M. R. *Langmuir* 2013, 29, (11), 3604-3609.
27. Cartier, E.; Stathis, J. H. *Microelectronic Engineering* 1995, 28, (1), 3-10.
28. Zeller, P.; Amati, M.; Sezen, H.; Scardamaglia, M.; Struzzi, C.; Bittencourt, C.; Lantz, G.; Hajlaoui, M.; Papalazarou, E.; Marino, M.; Fanetti, M.; Ambrosini, S.; Rubini, S.; Gregoratti, L. *physica status solidi (a)* 2018, 215, (19), 1800308.

Supporting Information

Sub-nanometer thin Conformal Aluminum Oxide Coating Created by Interconversion of SiO₂ *via* Hydrogen Plasma-assisted Atomic Layer Deposition

*Alex Henning^{§, +, *}, Johannes Bartl^{§, ‡, +}, Lukas Wolz[§], Maximilian Christis[§], Andreas Zeidler[§],
Michele Bissolo[§], Theresa Grünleitner[§], Johanna Eichhorn[§], Patrick Zeller^{†, #, %}, Matteo Amati[†],
Luca Gregoratti[†], Jonathan J. Finley[§], Bernhard Rieger[‡], Martin Stutzmann[§], Ian D. Sharp^{§, *}*

[§]Walter Schottky Institute and Physics Department, Technical University of Munich, 85748
Garching, Germany

[‡] Department of Chemistry, WACKER-Chair for Macromolecular Chemistry, Technische
Universität München, Lichtenbergstraße 4, 85747 Garching bei München, Germany

[†] Elettra-Sincrotrone Trieste SCpA, SS14-Km163.5 in Area Science Park, 34149, Trieste, Italy.

⁺These authors contributed equally

*sharp@wsi.tum.de, *alex.henning@wsi.tum.de

S1. Static contact angle measurements of Si substrates

Static contact angle (SCA) measurements were performed with the contact angle system OCA 15Pro (DataPhysics Instruments GmbH, Baden-Wuerttemberg, Germany) on Silicon substrates under ambient conditions (27.3 °C, 32.7 % relative humidity). Data were acquired and evaluated with the basic module SCA 20 - contact angle (DataPhysics Instruments GmbH, Baden-Wuerttemberg, Germany, ver. 2.0). To estimate an average Young-LaPlace contact angle, 1 μl of deionized H_2O (18.2 $\text{M}\Omega\cdot\text{cm}$ at 25 °C, Merck Millipore) was dispensed with a rate of 1 $\mu\text{l/s}$ from a high-precision syringe (Hamilton, DS 500/GT, gas-tight, 500 μl) on the sample surface and after ~ 3 s (reaching equilibrium) the side profile of the droplet was taken for further processing. SCAs from at least three different spots were determined to calculate a standard deviation (**Table S1**).

Table S1. Static water contact angle measurement on Silicon substrates before and after treatment (20 cycles TMA and H_2 plasma) in a plasma-enhanced ALD reactor. The thickness of the native oxide layer was determined by spectroscopic ellipsometry (SE).

substrate	SiO_2 thickness by SE	process details	water CA / °
Si/ SiO_2 / AlO_x	/	20 cycles TMA/ H_2 plasma process	24.7 ± 0.7
Si/ SiO_2	16 Å	Solvent-cleaned	64.0 ± 0.5

S2. Contact potential difference of Si substrates

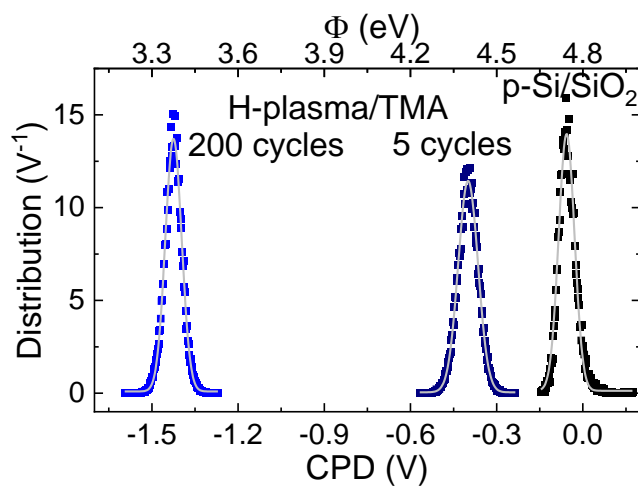


Figure S1. The TMA/H₂ process leads to a decrease in the contact potential difference (CPD) of the *p*-Si substrate, presumably due to an increase in the density of negative fixed charges at the SiO₂/AlO_x interface. The average CPD values were measured by Kelvin probe force microscopy and extracted from averaging 2×2 μm² (512 points sampling) images.

S3. X-ray photoelectron spectroscopy measurements of Si substrates

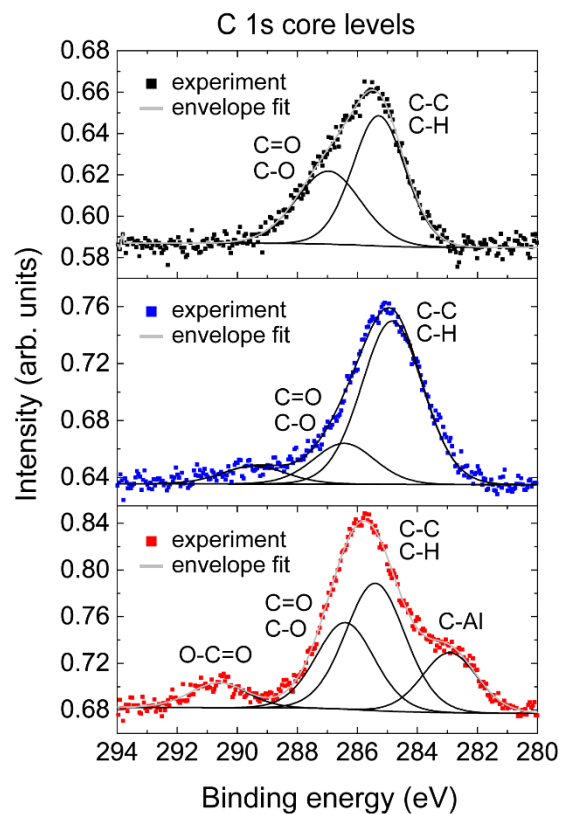


Figure S2. Carbon 1s core level spectra of solvent-cleaned bare *p*-doped Si (top, black squares), and *p*-Si substrates after exposure to 5 cycles (middle, blue squares) and 200 cycles (bottom, red squares) of TMA and H₂ plasma.

To provide further support for the presence of elemental aluminum on the surface of the Si substrate after ALD, we measured the Al KL_{2,3} L_{2,3} Auger spectrum using a magnesium X-ray source (Mg K_α = 1253 eV) with the XPS system described in the methods section of the main manuscript. Two main spectral features can be identified in the Al KLL Auger spectrum at kinetic energies of ~1386 eV and ~1393 eV (**Fig. S3**) and are attributed to aluminum oxide and elemental aluminum, respectively.¹ The peak energy separation of ~7 eV corresponds to reported binding energy separation between AlO_x and Al on aluminum foil.¹

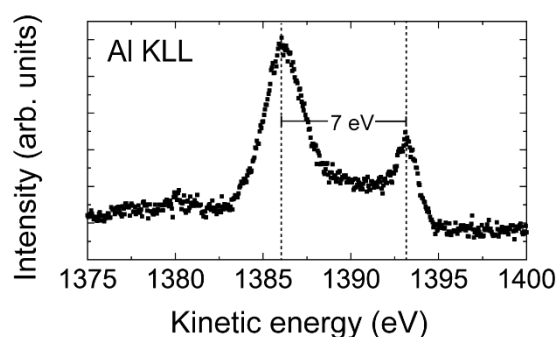


Figure S3. Corresponding Al KL_{2,3} L_{2,3} Auger spectrum of a Si substrate after TMA and hydrogen plasma treatment (200 cycles). The spectral feature at a kinetic energy of ~1393 eV and its separation from the dominant spectral feature at ~1386 eV indicate the presence of elemental aluminum.

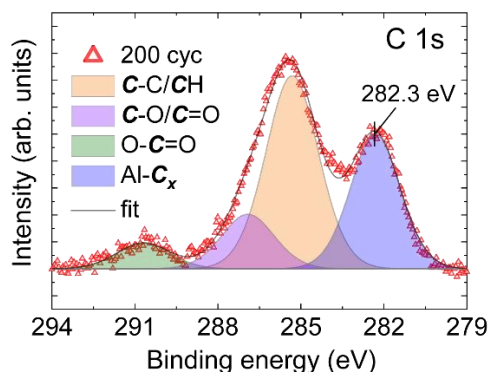


Figure S4. XPS spectra of the C 1s core level of a Si substrate after treatment with 200 cycles of the TMA/H₂ plasma process at 300 W plasma power and at 200 °C.

S4. Spectroscopic ellipsometry of Si substrates

We considered a three-layer model structure to analyze the SE spectra of a AlO_x film on a SiO_2 -coated Si substrate. To obtain the thickness of the SiO_2 layer, we first characterized a Si/ SiO_2 substrate without MoS_2 by SE. A temperature-dependent library model and the Sellmeier model were used to describe the optical properties of the silicon substrate and the SiO_2 layer, respectively.

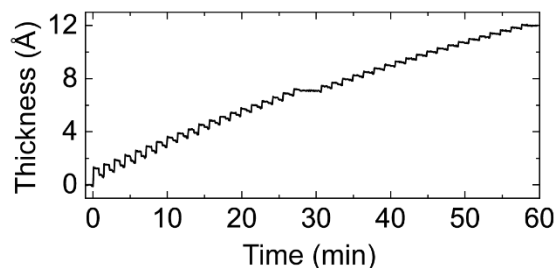


Figure S5. Thickness of AlO_x as a function of time plot obtained from *in-situ* SE on a *p*-doped Si substrate with a 270 nm thick thermal SiO_2 layer during 40 cycles of the TMA/ H_2 plasma process at 200 °C and 100 W plasma power.

REFERENCES

1. Buckley, A. N.; Hartmann, A. J.; Lamb, R. N.; Stampfl, A. P. J.; Freeland, J. W.; Coulthard, I. *Surface and Interface Analysis* **2003**, 35, (11), 922-931.